clean technologies

MDPI

Article

Zeolites for Secondhand Smoke Filtration: An Experimental Study on the Removal of Toxic Components from Cigarette Smoke and Comparison with Carbon Nanotubes (CNTs)

Luigi Madeo [1,*], Pietro Figliuzzi [2], Assunta Perri [3], Anastasia Macario [1], Carlo Siciliano [3,*] and Pierantonio De Luca [4,*]

[1] Dipartimento di Ingegneria per l'Ambiente, Università della Calabria, I-87036 Rende, Italy; anastasia.macario@unical.it
[2] Dipartimento di Fisica, Università della Calabria, I-87036 Rende, Italy; pietro.figliuzzi03@gmail.com
[3] Dipartimento di Farmacia e Scienze della Salute e della Nutrizione, Università della Calabria, I-87036 Rende, Italy; assunta.perri@unical.it
[4] Dipartimento di Ingegneria Meccanica, Energetica e Gestionale, Università della Calabria, I-87036 Rende, Italy
* Correspondence: luigi.madeo@unical.it (L.M.); carlo.siciliano@unical.it (C.S.); pierantonio.deluca@unical.it (P.D.L.)

Abstract

This study investigates the use of type A zeolite as a filtering material for the removal of toxic and carcinogenic compounds from cigarette smoke, which contains nicotine and other harmful substances produced by tobacco combustion. The aim is to evaluate the effectiveness of zeolite in reducing exposure to secondhand smoke, with particular attention to health and environmental impacts. The zeolite was characterized using SEM-EDS, XRD, DSC, and TGA to determine its morphology, chemical composition, crystalline structure, and thermal stability. An experimental setup was designed to simulate realistic smoking conditions and test filter efficiency based on the active mass. The system allowed identification of harmful substances trapped in the filter and those remaining in the air. Performance was assessed through gravimetric analysis and GC-MS, enabling identification of adsorbed and non-adsorbed compounds. Results demonstrate significant efficiency in selective removal of toxic components. Finally, filter performance was compared with carbon nanotubes, tested under the same experimental protocol.

Keywords: zeolite A; secondhand smoke; environmental tobacco smoke (ETS); adsorption kinetics; microporous materials; toxic organic compounds; air filtration; indoor air quality; carbon nanotubes (CNTs); environmental and human health

Check for updates

Academic Editor: Constantinos V. Chrysikopoulos

Received: 5 March 2026
Revised: 2 April 2026
Accepted: 7 April 2026
Published: 6 May 2026

Copyright: © 2026 by the authors. Licensee MDPI, Basel, Switzerland. This article is an open access article distributed under the terms and conditions of the Creative Commons Attribution (CC BY) license.

1. Introduction

The consumption of tobacco-containing products remains one of the leading preventable causes of mortality worldwide [1]. Despite the progressive decline in the number of smokers recorded in recent decades, it is estimated that more than one billion people still use tobacco, with an enormous health and social impact [2,3]. In addition to the direct harm caused by active smoking, the scientific community has increasingly focused on the effects of secondhand smoke, defined as the combination of emissions generated by cigarette combustion and the smoke exhaled by the smoker that disperses into the surrounding environment [4–6]. This complex aerosol, also known as environmental tobacco smoke, is now recognized as a major risk factor for non-smokers' health, contributing to the development of respiratory, cardiovascular, and oncological diseases.

Secondhand smoke consists of a heterogeneous mixture of solid and liquid particles suspended in a gaseous phase, generated by simultaneous processes of combustion, pyrolysis, distillation, and condensation occurring at temperatures between 800 and 900 °C [7–9]. The average particle size, typically around 0.2 µm, promotes prolonged suspension and diffusion in indoor environments, making removal through natural or mechanical ventilation difficult. The chemical composition of environmental tobacco smoke includes thousands of compounds, such as polycyclic aromatic hydrocarbons, aldehydes, volatile organic compounds, free radicals, nitrogen oxides, heavy metals, and nicotine [10–12]. The simultaneous presence of highly reactive and carcinogenic species makes secondhand smoke a significant threat even at low concentrations and during prolonged exposure.

In recent years, growing awareness of the risks associated with secondhand smoke has led to the adoption of various mitigation strategies, which can be broadly categorized into three main groups: regulatory interventions, behavioral interventions, and technological interventions [13]. Legislative policies—such as smoking bans in enclosed public spaces, workplaces, and near sensitive areas—have represented one of the most effective steps in reducing involuntary exposure [14,15]. However, such measures do not eliminate the problem in private environments, homes, vehicles, or crowded outdoor spaces, where direct control is more complex. Behavioral strategies, based on raising awareness among smokers and promoting safer practices, show variable effectiveness depending on the socio-cultural context.

On the technological front, several systems have been developed to reduce pollutants derived from tobacco smoke, including air purifiers, mechanical filters, activated carbon devices, and technologies based on ionization or photocatalysis [16–18]. However, many of these systems present significant limitations: high costs, frequent maintenance requirements, limited efficiency toward volatile organic compounds or free radicals, or poor selectivity for specific pollutant classes. Moreover, most commercial devices are designed to treat large air volumes, whereas secondhand smoke often concentrates in localized microenvironments, such as the area immediately surrounding a lit cigarette.

In this context, the use of porous materials with high adsorption capacity represents a promising strategy for the selective capture of toxic smoke components. In recent years, advanced materials such as carbon nanotubes (CNTs) have demonstrated high efficiency in the adsorption of pollutants [19–22]. Previous studies have shown that CNTs exhibit a strong affinity for many species present in cigarette smoke, due to their high specific surface area, nanostructured morphology, and unique electronic properties [23,24]. These findings have paved the way for the use of nanostructured materials in secondhand smoke filtration, highlighting the need to explore equally effective but more sustainable and cost-effective alternatives.

Research on microporous materials has revealed the potential of zeolites, crystalline materials characterized by a three-dimensional network of channels and cavities with molecular-scale dimensions [25–27]. They are widely used in catalysis, gas separation, and environmental processes, owing to their high surface area, ion-exchange capacity, and selectivity toward molecules of different polarity and size [28–30]. The systematic application of zeolites to the capture of secondhand smoke components remains relatively unexplored. Existing literature mainly focuses on industrial or catalytic applications, while only a limited number of studies specifically address cigarette smoke filtration under controlled and reproducible conditions [31,32].

The present work fits within this framework by proposing an experimental evaluation of the effectiveness of zeolites in removing toxic components from secondhand smoke, through a specifically designed setup aimed at simulating real emission and dispersion conditions. The objective is to provide an original contribution to the development of filtration systems based on microporous materials, capable of mitigating involuntary

exposure to environmental tobacco smoke and paving the way for future comparisons with other adsorbent materials, including the previously studied carbon nanotubes.

2. Materials and Methods

The experimental work was systematically designed to evaluate the effectiveness of zeolites in retaining the chemical species released during cigarette combustion, with particular attention to toxic organic compounds and volatile fractions. To this end, a dedicated laboratory system was assembled, capable of reproducing controlled and reproducible conditions for smoke generation and conveyance. A dual-stage filtration system was constructed, designed to distinguish between substances fully adsorbed by the active material and those not retained and dispersed in the outlet flow. Commercial standardized cigarettes were used as the emission source to ensure uniform smoke production and comparability across different experimental trials.

The following sections provide a detailed description of the materials employed, the configuration of the experimental apparatus, the operational parameters adopted, and the analytical procedures used for chemical characterization and performance evaluation of the filtration system.

2.1. Experimental Apparatus

A custom-built system was used to generate and convey cigarette smoke under controlled conditions (Figure 1). The experimental apparatus consisted of: a custom water-based vacuum pump, assembled in the Chemistry Laboratory at the University of Calabria (Rende, Italy), providing continuous suction; a custom L-shaped metal holder, assembled in the same laboratory, with the horizontal part connected via a PVC tube (PVC tube, 0.5 cm diameter, Guanghai Electronic Insulation Material Co., Ltd., Shenzhen, China) to the vacuum line and the vertical part holding the cigarette in a vertical position, simulating "human" combustion and directing the smoke toward the air pump; a plexiglass combustion chamber custom-built in the laboratory (Chemistry Laboratory, University of Calabria, Rende, Italy) with access ports; a primary filter containing zeolites A (Sigma-Aldrich Co. LLC, Merck Group, Burlington, MA, USA), an upstream cellulose filter (Brand, New York, NY, USA), and a secondary electric air pump (Jsdoin, model CZ-198C, Shenzhen, China) maintaining constant flow through the entire system, allowing sample collection for subsequent chemical analyses as described throughout the study.

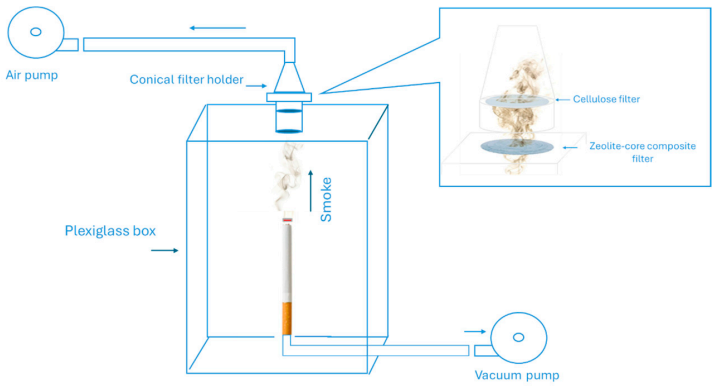

Figure 1. Schematic of the experimental apparatus used for cigarette smoke generation and conveyance. The flow (indicated by arrows) starts from the water-based vacuum pump (right), passes through the L-shaped metal holder that maintains the cigarette in a vertical position, enters the plexiglass combustion chamber (with closed access port), and is drawn by the secondary air pump through the primary filter containing zeolites and the upstream cellulose filter. The cigarette is ignited and allowed to burn to completion; the process is repeated three times for each sample, ensuring reliable sample collection and scientific analysis.

The chamber is not insulated and allows air to enter through the natural micro-fissures of the structure, enabling cigarette combustion. The negative pressure generated by the suction pump directs the smoke toward the filter, preventing dispersion and ensuring reproducible experimental conditions.

This configuration ensured stable combustion and minimized variability associated with human smoking behavior.

2.2. Zeolites

The zeolites used in this study were selected based on their microporous structure and thermal stability, characteristics that make them suitable for interacting with the volatile and particulate species present in cigarette smoke. The material consisted of a type A zeolite, chosen for its well-defined pore architecture and its widespread use in adsorption applications.

Prior to use, the zeolite was morphologically and structurally characterized (see Results) to confirm its suitability for the experimental conditions. The zeolite A used in this study is a commercial material widely characterized in the literature and available as a certified reference (NIST RM 8851). Typical values include a BET specific surface area of 20–30 m^2/g, a pore volume of 0.25–0.30 cm^3/g, and micropores with openings of about 4 Å, characteristic of the LTA structure.

To promote uniform particle dispersion and enhance access to the active surfaces, the material was sonicated in distilled water for 15 min at a frequency of 40 kHz using an ultrasonic bath. This treatment allowed for the preparation of a homogeneous suspension and reduced possible aggregates, thereby optimizing the adsorptive properties of the material during the experimental tests.

2.3. Experimental Filter Tips

The filtration system consisted of two elements arranged in series. The primary filter was prepared by distributing known masses of zeolites between two circular sheets of filter paper (11 µm, ϕ = 55 mm, Cat. No. 1001055, Whatman, (Cytiva), Marlborough, MA, USA). The edges of the disks were sealed to prevent material loss during smoke suction. The resulting disk-shaped filter was compact, mechanically stable, and easy to handle (Figure 2). Four versions were produced, containing 0 g (blank), 0.03 g, 0.06 g, and 0.09 g of zeolites. These masses were selected based on preliminary trials aimed at identifying a suitable range compatible with the filter geometry and the expected smoke flow, while ensuring uniform distribution of the adsorbent material.

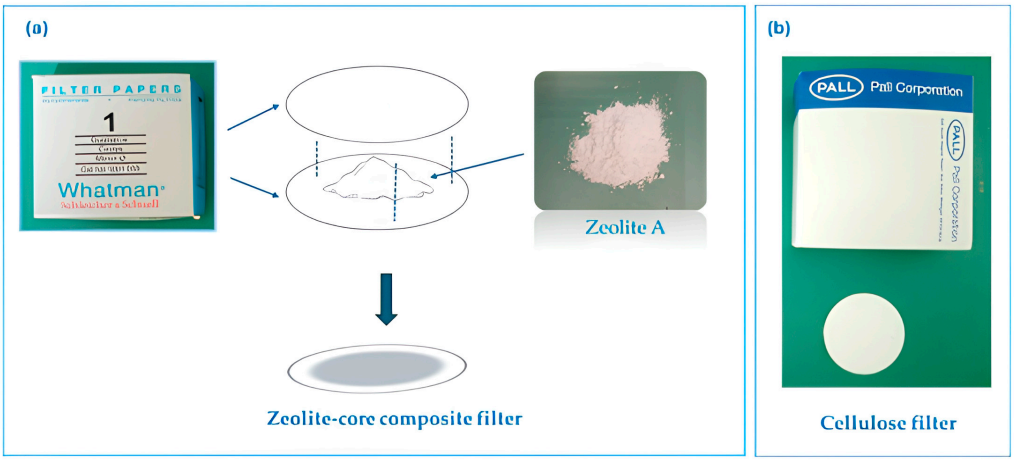

Figure 2. (**a**) Preparation of the zeolite-core composite filter. The dotted arrows indicate the assembly process, where zeolite is placed between two paper filters and then sealed together. The blue arrow shows the final appearance of the zeolite-containing filter. r; (**b**) Cellulose filter.

Upstream of the zeolite filter, a cellulose filter commonly used for atmospheric particulate sampling (Figure 2b) was placed to collect any particles not retained by the primary element. This dual-stage configuration allows a quantitative distinction between species effectively adsorbed by the microporous material and residual particles, improving the assessment of the system's filtration efficiency. The filters were assembled under controlled conditions to minimize particle dispersion and ensure reproducibility across experimental trials.

2.4. Commercially Available Cigarette

To ensure reproducible and standardized combustion conditions, commercial cigarettes from a widely distributed national brand were used. The selection of a standardized industrial product allowed for the minimization of variability related to tobacco composition and construction features, ensuring uniformity across experimental trials. The type used was king size, blue version; the declared values for this type of cigarette are approximately: nicotine ~1.0 mg, tar ~12 mg, and carbon monoxide ~12 mg per single cigarette.

Each cigarette (Figure 3) consists of a cellulose acetate filter, designed to retain a portion of the particles and chemical compounds generated during combustion; a specially formulated wrapping paper, which regulates burn rate, controls air permeability, and ensures uniform combustion along the length of the cylinder; and a cylinder of shredded and compacted tobacco, which serves as the main source of smoke emission and volatile chemical species.

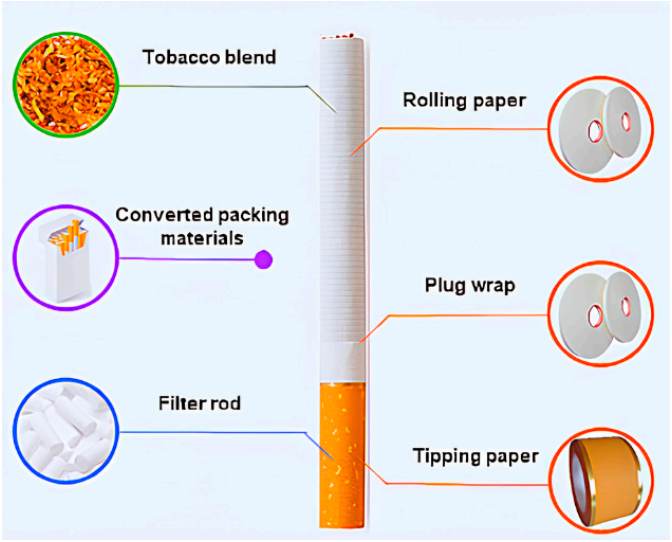

Figure 3. Schematic of a commercial cigarette. The illustration highlights the internal structure and the arrangement of the main components.

This configuration reflects industrial standards and guarantees reproducibility of smoke emission conditions, which is essential for the comparative evaluation of the experimental filtration materials. Standardizing the cigarette reduces variations due to differences in tobacco density, moisture content, or cigarette construction, thereby improving the reliability of the data collected during the filtration tests.

2.5. Experimental Procedure

For each filter configuration, three cigarettes were combusted, and the reported values represent the average of the measurements. Before testing, all filters were conditioned for 24 h in a desiccator containing silica gel and weighed using a five decimal analytical balance. After exposure to smoke, each filter was reweighed to determine the mass of retained material. The cigarette was placed in the holder, the filters were inserted into

their housings, and the pumps were activated. Combustion proceeded until the cigarette's built-in filter was reached. Residual smoke was drawn for approximately one minute before shutting down the system. Each experimental cycle (three cigarettes) was repeated three times using new filters and a constant zeolite mass. The system was calibrated so that each cigarette was consumed in a constant time of approximately 2.5 min, ensuring the repeatability of the tests and simulating a typical act of consumption by a smoker.

2.6. Adsorbate Extraction and Sample Preparation

To recover the chemical species adsorbed on the filters, a general extractive procedure based on Deep Eutectic Solvents (DESs) was employed. Following the previously described method [24], all extracts were obtained by treating the respective zeolite or cellulose filters with 0.5 mL of freshly prepared DES. The DES was prepared by mixing choline chloride and ethylene glycol in a 1:2 molar ratio and heating the mixture at 70 °C under magnetic stirring until a homogeneous liquid formed. An equal volume of distilled water (0.5 mL) was added to facilitate solubilization, and the mixtures were sonicated for 15 min at 25 °C in an ultrasonic bath to ensure uniform extraction. After sonication, the suspensions were centrifuged and treated with 1 mL of methyl tert-butyl ether. The resulting organic phases were collected, and 1 µL aliquots were injected into a Gas Chromatography–Mass Spectrometry (GC–MS, Bruker, Billerica, MA, USA) system for chemical analysis.

Morphological and structural characterization of the zeolites was performed using a scanning electron microscope (ESEM Quanta 200 FEG, FEI Company, Eindhoven, The Netherlands). The particulate fraction retained by the filters was quantified gravimetrically using a five-decimal analytical balance (OHAUS ANALYTICAL Plus, OHAUS Corporation, Parsippany, NJ, USA).

GC–MS analyses were carried out on a Hewlett Packard system equipped with a polysiloxane-coated capillary column (30 m × 0.25 mm i.d. × 0.25 µm). Helium was used as the carrier gas at a flow rate of 1 mL/min. Mass spectra were acquired in electron impact mode at 70 eV. A 1 µL aliquot of each extract was injected in splitless mode to maximize analyte transfer onto the column. The oven program started at 60 °C (isothermal for 2 min) and was then ramped at 20 °C/min to a final temperature of 280 °C. This configuration enabled the detection and characterization of volatile and semi-volatile organic compounds by GC–MS, providing comprehensive molecular profiles of the species adsorbed by both zeolite and cellulose filters.

3. Results and Discussion

The following sections present the preliminary characterization of the zeolite, performed to evaluate its structural, morphological, and thermal properties relevant to the adsorption of species present in cigarette smoke. FTIR analyses were carried out to identify functional groups, while DSC-TGA measurements were employed to assess thermal stability and the material's behavior under heating.

Subsequently, the experimental data obtained from the filters are reported. Gravimetric and colorimetric analyses were used to quantify the particulate fraction retained, while Gas Chromatography–Mass Spectrometry (GC–MS) provided detailed information on the volatile and semi-volatile species adsorbed.

Finally, the results obtained with the zeolite-based filters are compared with data from a previous study conducted under the same experimental conditions using carbon nanotubes (CNTs). This comparison highlights differences in adsorption efficiency and selectivity toward the various chemical components of smoke, allowing an assessment of the potential of zeolites as a sustainable and high-capacity adsorbent alternative to previously studied nanostructured materials.

3.1. Characterization of Zeolite A as an Adsorbent Material in Filters

3.1.1. XRD and FTIR Characterization

The following image (Figure 4) shows the XRD diffractogram of zeolite A used prior to the experimental tests. This analysis was carried out in order to verify the crystalline nature of the material and to confirm its belonging to the A-type structure. The diffractogram, which represents the distribution of diffraction angles as a function of peak intensity, highlights the characteristic reflections typical of zeolite A, thus enabling precise identification of its crystalline structure. This confirmation is essential to ensure that the material used in the experiments is the intended one and that its adsorptive properties correspond to the expected performance.

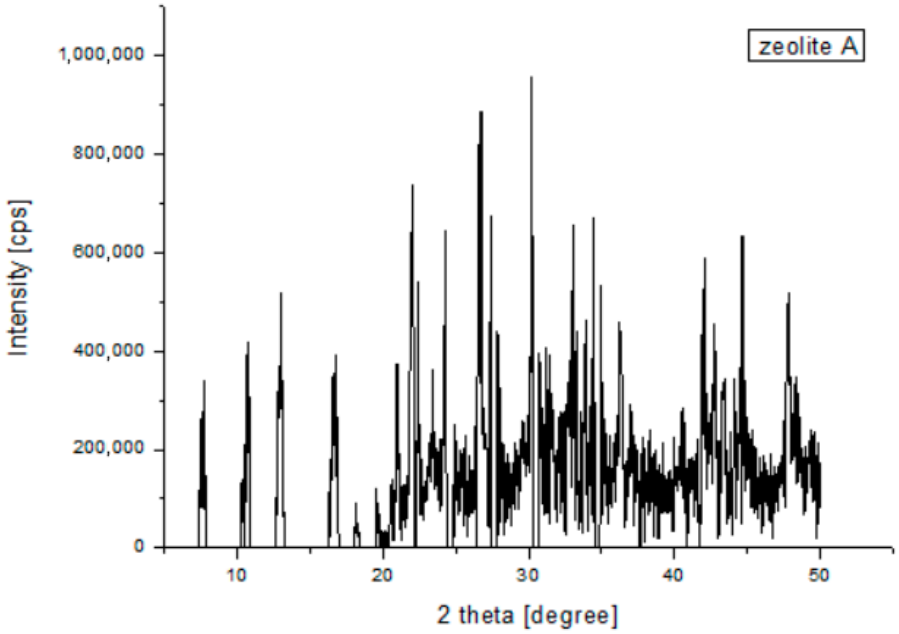

Figure 4. XRD spectrum of the zeolite used.

The X-ray diffraction spectrum (Figure 4) shows a series of well-defined and relatively sharp peaks, fully consistent with the characteristic pattern of A-type zeolite (LTA structure), indicating a high degree of crystallinity and good phase purity of the material, with no significant evidence of secondary crystalline phases.

The FTIR spectrum (Figure 5) highlights the main characteristic bands associated with the aluminosilicate framework and the intrinsic microporosity of the material. Zeolites are crystalline aluminosilicates composed of a three-dimensional network of SiO_4 and AlO_4 tetrahedra interconnected through shared oxygen atoms. This structural arrangement gives rise to a distinctive FTIR profile, in which lattice vibrations, framework-related bands, and signals attributed to adsorbed species—particularly water molecules—can be clearly identified. The most significant absorption bands are summarized in Table 1, together with their corresponding structural assignments.

In the FTIR spectrum of the analyzed sample, the band observed at approximately 1672 cm^{-1} is attributed to the δ(H–O–H) bending vibration of physically adsorbed water molecules located within the channels and cavities of the zeolite. This signal is typical of zeolitic materials and confirms the pronounced hydrophilic nature of the aluminosilicate framework, while also indicating that the sample was not completely dehydrated under the analysis conditions. This band is generally accompanied by a broad O–H stretching band in the 3400–3600 cm^{-1} range, associated with hydrogen-bonded water; in the present spectrum, this contribution appears weak, suggesting a moderate water content or less extensive hydrogen-bonding interactions. The most intense bands are located in the

1200–900 cm^{-1} region, characteristic of the asymmetric stretching vibrations of T–O–T bridges (T = Si, Al) forming the aluminosilicate framework. In particular, the peak centered at approximately 1005 cm^{-1} is assigned to the asymmetric stretching of Si–O–Si and Si–O–Al bonds. The position of this band, close to 1000 cm^{-1}, indicates significant aluminum incorporation into the crystalline network and suggests a medium-to-low Si/Al ratio, consistent with A-type zeolite. An additional intense band observed at approximately 962 cm^{-1} is attributed to the stretching of Si–O–Al bonds associated with AlO_4^- tetrahedra. This vibration is directly related to the presence of negative charges within the framework, whose electrical neutrality is balanced by extra-framework cations (e.g., Na^+, K^+, or Ca^{2+}). The high intensity of this band indicates a substantial concentration of structural aluminum and is commonly associated with high ion-exchange capacity and potential catalytic properties of the zeolite. Bands in the 800–400 cm^{-1} region are attributed to lattice vibrations. In particular, signals around ~650 cm^{-1} are associated with symmetric T–O–T vibrations and structural ring deformation modes. The well-defined bands at approximately 560 cm^{-1} correspond to vibrations of double four-membered or six-membered rings (D4R or D6R), considered "fingerprint" bands of zeolitic structures. Their presence and definition confirm a high degree of crystallinity and structural order of the framework.

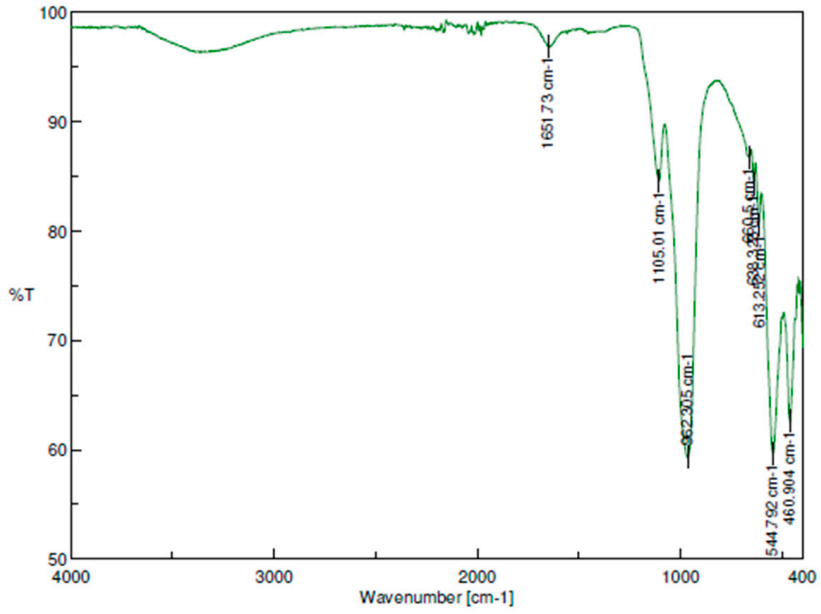

Figure 5. FTIR spectrum of A-type zeolite.

Table 1. FTIR Band Assignment of the Zeolite Sample.

Peak (cm^{-1})	Vibrational Mode/Bond	Structural Origin
~1672	H–O–H bending vibration	Adsorbed water
~1005	Asymmetric Si–O–Si/Si–O–Al stretching	Aluminosilicate framework
~962	Si–O–Al stretching (AlO_4^- units)	Framework active sites
~650	Symmetric T–O–T ring vibrations (T = Si, Al)	Framework lattice
~560	Double-ring vibrations (D4R/D6R)	Zeolite fingerprint band

Overall, the analyzed FTIR spectrum is fully consistent with that of a crystalline A-type zeolite, characterized by a well-developed Si–O–Al framework, the presence of adsorbed water within the micropores, and diagnostic bands indicative of a highly ordered zeolitic structure.

3.1.2. Morphological and Elemental Characterization by SEM-EDS

The A-type zeolite used in this study was characterized by scanning electron microscopy (SEM). SEM images revealed that the sample consists of crystals exhibiting the characteristic cubic morphology typical of A-type structures. Although the crystal geometry is generally uniform, the particles show a noticeable size variation: the observed crystal edges range approximately from 460 nm to 3.3 µm, indicating a relatively broad particle size distribution, consistent with commercial materials not fractionated by size. The crystal surfaces appear well-defined, smooth, and free of macroscopic defects, indicating a high degree of crystallinity and structural integrity (Figure 6). These morphological features are consistent with the expected adsorptive properties of A-type zeolite and suggest that the material possesses good quality for filter applications.

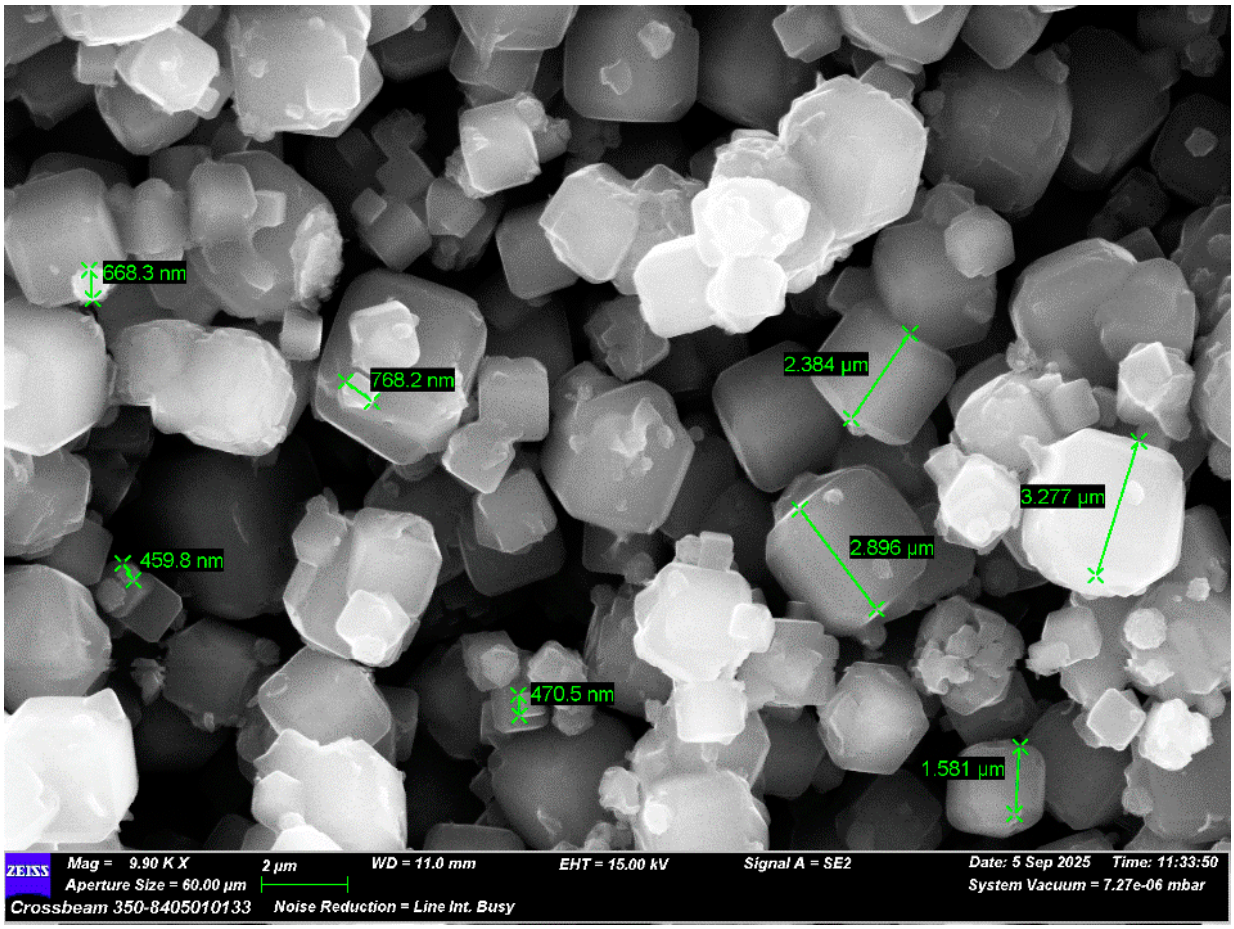

Figure 6. SEM image showing the morphology of A-type zeolite crystals.

EDS analysis performed on the regions observed by SEM confirmed the elemental composition of the material, showing a predominance of oxygen, aluminum, and silicon in ratios consistent with the structure of A-type zeolite. Both the spectrum and qualitative elemental mapping revealed no significant impurities, thereby confirming the high purity of the sample used (Figure 7).

The EDS spectrum reveals a predominance of oxygen, along with well-defined signals for sodium, aluminum, and silicon, which constitute the SiO_4/AlO_4^- tetrahedral framework characteristic of A-type zeolite. The absence of significant amounts of foreign elements indicates that the material does not contain notable secondary inorganic phases, confirming its high compositional purity.

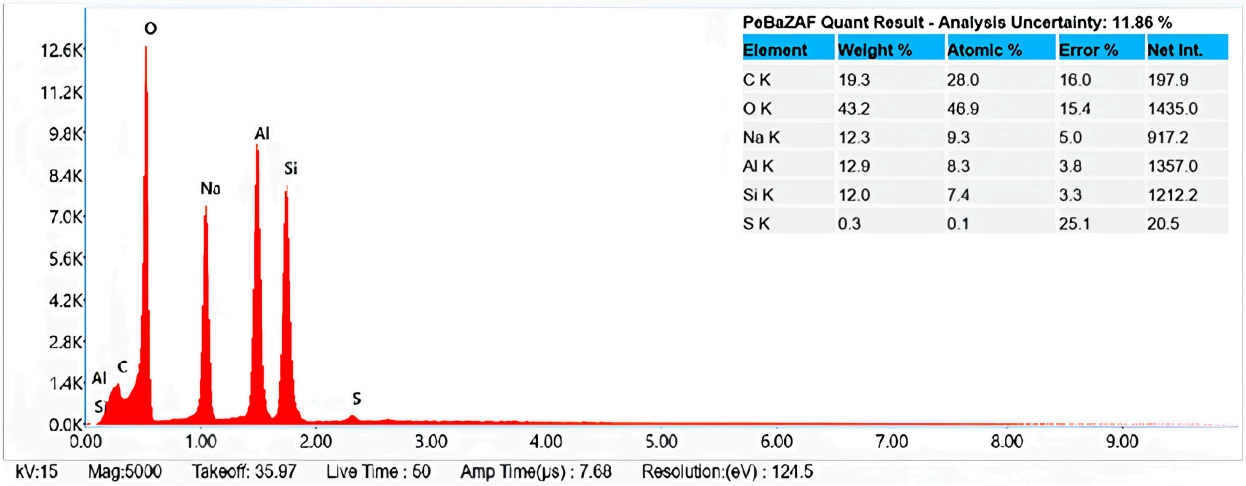

Figure 7. Energy-dispersive X-ray spectroscopy (EDS) spectrum of A-type zeolite, showing its elemental composition.

The carbon signal, although appearing with noticeable intensity, can be attributed entirely to sample preparation (e.g., support material or superficial residues) and does not represent a structural component of the zeolite. Such contributions are common in EDS analyses of porous materials and do not affect the chemical interpretation of the sample.

Consistent with the XRD analysis, the sample is highly crystalline and corresponds to the LTA structure. However, despite the presence of a sharp and characteristic diffractogram, the existence of minor amorphous or partially ordered fractions cannot be completely excluded, likely below the detection limit of the technique.

Overall, the EDS results are fully consistent with the diffraction data, confirming both the composition and high quality of the analyzed material.

3.1.3. Thermal Characterization by DSC and TGA

The analyzed sample is an aluminosilicate zeolite, whose morphology was preliminarily evaluated using scanning electron microscopy (SEM). The images reveal a crystalline structure typical of zeolitic materials, featuring well-defined cavities and channels indicative of a certain microporosity, although no quantitative measurement of the specific surface area or pore size distribution was performed.

To investigate the thermal behavior of the material and assess the stability of the framework, a combined TGA–DSC analysis was carried out (Figure 8). TGA allows the identification and quantification of mass losses associated with dehydration and dihydroxylation processes, while DSC detects endothermic events related to water evaporation and potential structural transformations. The integration of TGA and DSC data thus provides a comprehensive understanding of the thermal behavior of the zeolite, essential for evaluating its stability and potential applications.

The thermal characterization of the zeolite sample, performed using TGA and DSC, reveals a sequence of physical and chemical processes typical of microporous aluminosilicate materials. The TGA curve initially shows, between 25 and 150 °C, a minor mass loss (~5%), attributable to the removal of physically adsorbed water on the crystal surfaces, without significant structural alterations.

A second critical interval occurs between 150 and 350 °C, where the most pronounced mass loss (~15–20%) corresponds to the dehydration of intracrystalline water contained within the zeolite channels and cavities. Partial dehydroxylation of –OH groups may also begin in this range, while the crystalline structure remains largely stable. Beyond 350 °C and up to approximately 700 °C, the mass loss progresses more gradually (~5%), reflecting

complete dehydroxylation and the onset of framework reorganization, with progressive loss of crystallinity above 500–600 °C. At the end of the analysis, approximately 75% of the initial mass remains, indicating a total volatile fraction of ~25%.

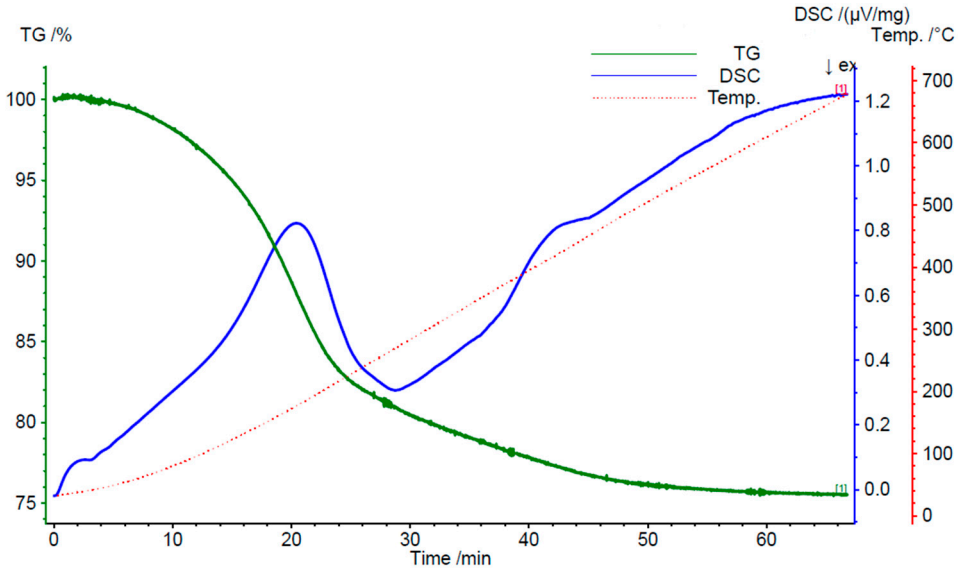

Figure 8. Thermogravimetric (TGA) and differential scanning calorimetry (DSC) analysis of the zeolite used as filter material. The left y-axis (green) represents TGA in (%); the x-axis (black) shows time in (minutes); the right y-axis (blue) indicates DSC in (µV/mg); the temperature ramp is shown in red (°C), with the numerical indication provided directly by the instrument for the secondary axis.

The DSC curve complements the TGA data. A prominent endothermic peak between 200 and 250 °C corresponds to the evaporation of intracrystalline water, consistent with the rapid mass loss observed in TGA. Between 350 and 500 °C, a broader, less defined endothermic event is observed, attributable to dehydroxylation processes and internal reorganization of the zeolite lattice. Above 600 °C, the curve exhibits a continuous endothermic increase, indicative of energetically absorbing phenomena such as the onset of amorphization, loss of crystallinity, and possible high-temperature phase transitions. The absence of exothermic peaks throughout the analyzed range confirms the inorganic nature of the sample and the lack of oxidizable organic components.

In summary, the combined TGA–DSC analysis demonstrates that the zeolite exhibits high thermal stability up to approximately 300–350 °C, with mass loss limited to adsorbed and intracrystalline water. Above this threshold, progressive dehydroxylation and framework reorganization occur, leading to partial amorphization at temperatures approaching 700 °C. The residual mass of 75% confirms the strongly inorganic character of the material and the robustness of the siliceous-alumina framework. Overall, the thermal behavior is consistent with that of natural and synthetic zeolites, characterized by a high capacity to retain water within the channels and good structural stability at moderate to high temperatures.

3.2. Macroscopic Observation of Filters Incorporating Zeolite

No aggregation or cluster formation was observed in filters containing A-type zeolite: the particles were uniformly dispersed within the filter bed, occupying a small volume and retaining considerable mobility even in the configuration with a total mass of 0.09 g. Macroscopically, the degree of darkening of the cellulose filter overlaying the zeolite layer decreases with increasing zeolite content (Figure 9).

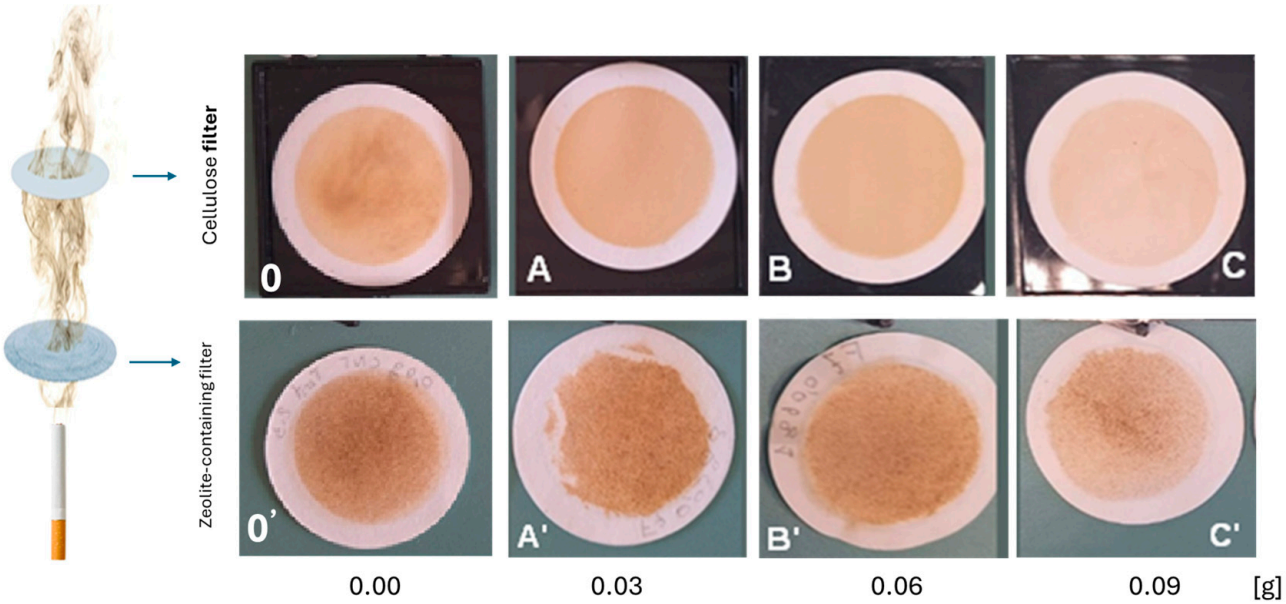

Figure 9. Visual comparison of cellulose filters and zeolite-core composite filters with different zeolite loadings. The cellulose filters on the top are labeled 0, A, B, and C; the corresponding zeolite-containing filters at the bottom are labeled 0′, A′, B′, and C′.

Compared to the blank test, conducted without any adsorbent material, filters containing 0.03 g and 0.06 g of zeolite exhibit only slight lightening, whereas the 0.09 g configuration results in a visibly lighter cellulose filter. This behavior suggests that higher amounts of zeolite are capable of retaining a larger fraction of the volatile and semi-volatile components present in the smoke, thereby reducing the darkening of the cellulose filter. These preliminary observations provide a qualitative basis for subsequent gravimetric and colorimetric analyses, which are necessary for a more accurate assessment of the zeolite's effectiveness in capturing species from the smoke.

3.3. Gravimetric Analysis

Gravimetric tests conducted on the cellulose filters indicate that the retention efficiency of volatile components depends not only on the amount of zeolite present in the filter bed, but is also strongly influenced by its distribution within the filter and the degree of material compaction. A uniform distribution promotes greater contact between the smoke and the adsorbent particles, enhancing the capture of volatile and semi-volatile species. Conversely, regions of particle accumulation or agglomeration may reduce pore accessibility and, consequently, the overall filtration efficiency. Figure 10 illustrates how variations in zeolite loading, combined with differences in the internal structure of the filter, can significantly affect the final retained mass, highlighting the importance of both adsorbent quantity and spatial arrangement in determining filter performance.

The weight gain of the cellulose filter coupled with the cartridge containing 0.03 g of zeolite was higher than that observed for cartridges containing 0.06 g and 0.09 g. All reported values represent the average of three independent experiments conducted under identical conditions, ensuring both repeatability and reliability of the results. A significant observation from the measurements is that all cellulose filters associated with zeolite-containing cartridges exhibit a systematically higher weight than the corresponding blank filters, regardless of the amount of zeolite employed. This behavior, seemingly contradictory and contrary to expectations—which predicted a decrease in filter weight compared to the blank—can be attributed to the presence of residual amorphous material and fine particulate matter within the zeolites. Although preliminary sonication reduces the amount of these particles, it does

not completely eliminate them; the residual fraction may also vary depending on the zeolite mass and the effectiveness of the treatment. During smoke passage, part of this material is released from the cartridge and subsequently captured by the cellulose filter, resulting in a weight increase exceeding that observed for the filter associated with the blank cartridge. An additional factor contributing to the weight gain of filters coupled with the 0.03 g and 0.06 g cartridges is the lower compaction of the zeolite bed. Since the volume of the composite filter remains constant, a lower mass results in a more porous and discontinuous structure, promoting smoke channeling. Under these conditions, the smoke can follow preferential paths, partially bypass the first filtration stage, and reach the cellulose filter, further increasing its weight. Conversely, in 0.09 g cartridges, the higher mass produces a more compact and homogeneous bed, reducing the formation of preferential channels and improving the efficiency of the first filtration stage.

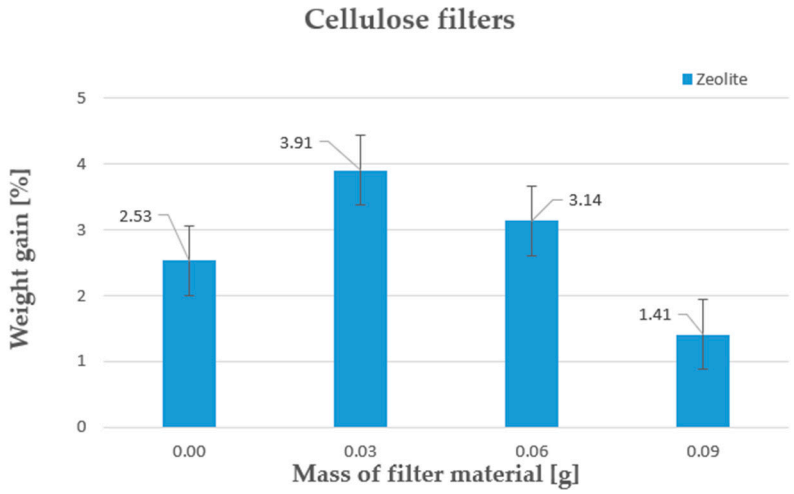

Figure 10. Weight gain of cellulose filters as a function of the zeolite mass contained in the pads. Measurements are affected by an error of ±0.01 g.

These results clearly demonstrate that gravimetric measurements alone are insufficient to accurately assess the effectiveness of zeolites in retaining particulate matter generated from cigarette smoke. The contribution to the weight gain due to residual amorphous material—which cannot be completely removed even after sonication and cleaning—is comparable to or even greater than the actual particulate generated by combustion. Since the particulate produced by smoke is relatively minor compared to the amorphous fraction released by the zeolites, the overall gravimetric signal is dominated by the latter, making it difficult to isolate and quantify the actual filtration contribution of the zeolites.

Thus, the potential of zeolites to retain volatile components generated during combustion remains unresolved. This phenomenon cannot be evaluated via gravimetric analysis, as volatile compounds contribute negligibly to the filter weight. Their retention can only be determined through gas chromatographic analyses, which allow selective identification and quantification of volatile and semi-volatile species. This approach, detailed in the following section, represents the only reliable method to determine the actual capacity of zeolites to adsorb volatile compounds present in cigarette smoke.

3.4. Comparative Assessment of Gravimetric Performance: Zeolite vs. Carbon Nanotube Filters

This section presents a comparison between carbon nanotubes (CNTs) tested under the same experimental conditions, with results already reported in our recent publication [24], and the zeolite employed in the present study (Figure 11). The aim is to evaluate how the nature of the filter material affects the weight gain of the cellulose filter, a parameter that reflects the system's ability to retain particulate matter generated during combustion.

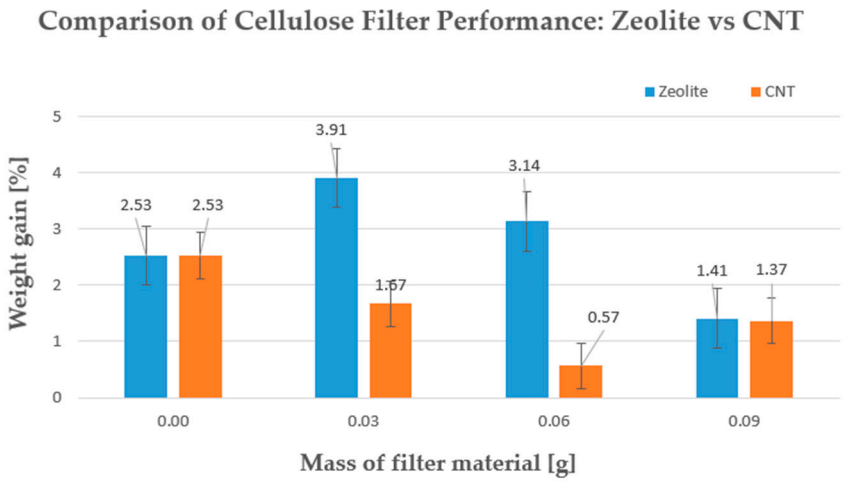

Figure 11. Comparison of the weight gain of cellulose filters paired with different types of adsorbent materials, plotted as a function of the amount of material loaded in the composite filter bed. Measurements are affected by an error of ±0.01 g.

As discussed in the previous section, cellulose filters coupled with cartridges containing zeolite exhibit a systematically higher weight gain compared to the blank filter (≈2.5%). This behavior is attributed to the release of a residual amorphous fraction and fine particulate matter, which cannot be completely removed even after sonication. Since sonication did not completely remove the amorphous component, future developments may involve repeating multiple treatment cycles, calibrated to the amount of zeolite in order to limit material loss. Alternatively, the literature also suggests complementary approaches, such as mild chemical washing or post-synthesis hydrothermal treatments, which could further reduce the residual amorphous fraction. During smoke passage, part of this material is released and subsequently captured by the cellulose filter, significantly contributing to the gravimetric gain and making it difficult to isolate the actual contribution of combustion-generated particulate matter.

Additionally, in cartridges containing 0.03 g and 0.06 g of zeolite, the lower compaction of the zeolite bed promotes channeling phenomena, allowing smoke to bypass part of the first filtration stage and reach the cellulose filter more easily. Only in the 0.09 g cartridges does the higher mass result in a more compact and homogeneous bed, reducing the formation of preferential paths and producing a gravimetric gain comparable to the blank filter (≈1.5%).

The behavior of carbon nanotubes (CNTs) is markedly different. Filters coupled with CNT-containing cartridges show a pronounced decrease in weight gain as the filter mass increases up to 0.06 g, dropping from ≈1.7% to ≈0%. This configuration represents the most efficient among all tested setups, achieving the lowest gravimetric gain. At 0.09 g, a slight increase is observed (≈1.5%), suggesting a potential efficacy limit beyond a certain material threshold or a modification in the filter bed structure. In direct comparison, it is evident that CNTs provide superior performance relative to zeolites in the removal of solid particulate matter. While in zeolite-based filters the gravimetric signal is dominated by the release of residual amorphous material, in CNT filters the weight gain more accurately reflects the true ability to retain combustion-generated particulate matter. This distinction highlights CNTs as a significantly more reliable material for evaluating the efficiency of the first filtration stage.

Finally, it remains to be determined whether zeolites can be effective in adsorbing volatile components of smoke—a phenomenon that cannot be assessed through gravimetric measurements. Evaluation of this capability requires gas chromatographic analyses,

described in the following section, which constitute the only reliable method to determine the actual capacity of zeolites to capture volatile and semi-volatile species.

3.5. Gas Chromatography–Mass Spectrometry Analysis of Smoke Samples: Comparison Between Zeolite and Carbon Nanotube Filters

This section presents the qualitative analyses performed to characterize the molecular profile of the extracts obtained from zeolite-containing filters and the corresponding cellulose filters used under identical experimental conditions. Analyses were carried out using gas chromatography coupled with mass spectrometry (GC–MS), with each measurement performed in triplicate to ensure repeatability and reliability. Identification of organic compounds was achieved by electron impact (EI) mass spectrometry and subsequently confirmed through comparison of the acquired spectra with reference data available in major spectral libraries (Wiley 8 and Wiley Fragrances). All samples subjected to instrumental analysis were prepared according to the previously described experimental procedure. For each chromatographic run, 1 μL aliquots of the final extract solutions were injected. The analytical method consisted of a total run time of 57 min, employing a temperature program ranging from 60 °C to 280 °C, using a polysiloxane-based capillary column.

This approach enabled effective separation of volatile and semi-volatile species present in the extracts, allowing reconstruction of the molecular profile of the analyzed samples.

GC–MS Analysis of the Cellulose Filter and Zeolite Core Composite Filter

The chromatographic runs are presented in their original form, exactly as generated by the instrument software, to preserve the integrity of the profiles and retention times; reducing the figures would have resulted in the removal of significant portions of the chromatogram. Figures 12 and 13 report the chromatographic runs corresponding to an experiment carried out using the zeolite-containing filter. Specifically, Figure 12 shows the chromatogram obtained from the injection of the extract derived from the zeolite filter, whereas Figure 13 illustrates the chromatogram corresponding to the extract obtained from the cellulose filter used in the same experiment. The pair of chromatograms presented refers to the experimental configuration that exhibited the best performance according to the gravimetric analysis and therefore represents the most significant case for qualitative comparison of the molecular profiles. To facilitate data interpretation, the images have been appropriately zoomed in on selected chromatographic regions of interest. This adjustment allows clearer visualization of the diagnostic peaks and highlights differences in the distribution of volatile and semi-volatile species between the two samples, thereby improving the scientific interpretation of the results and the overall significance of the study.

This approach enables a more accurate qualitative assessment of the effect of the zeolite on the molecular composition of the smoke, emphasizing variations in the presence and relative intensity of specific organic compounds.

The GC–MS analysis of the extract obtained from the zeolite-based filter (Figure 12) reveals a molecular profile primarily composed of the main classes of organic compounds typically present in cigarette smoke. As shown in the chromatographic plot, the retained substances include nicotine, aliphatic and unsaturated hydrocarbons (e.g., tetradec-1-ene and heptadecene), nitrogen-containing heterocyclic derivatives, phthalates, and long-chain alcohols. Nicotine (peak 4) and phthalic acid (peak 29), two compounds known for their high toxicological relevance, were selected as non-specific markers to evaluate the adsorption efficiency of the zeolite. Nicotine generates one of the most intense peaks in the chromatogram, indicating that the zeolite is capable of adsorbing it to a significant extent, although at a lower level compared to phthalic acid, which corresponds to the base peak of the chromatogram. With reference to the chromatogram obtained from the injection of the extract derived from the cellulose filter used in the same experiment (Figure 13), the nicotine peak appears very

intense (peak 3), whereas phthalic acid is not detectable within the instrumental sensitivity limits. In this case, the presence of nicotine suggests that the zeolite is not able to completely retain this compound, while it appears to be more effective in adsorbing phthalic acid.

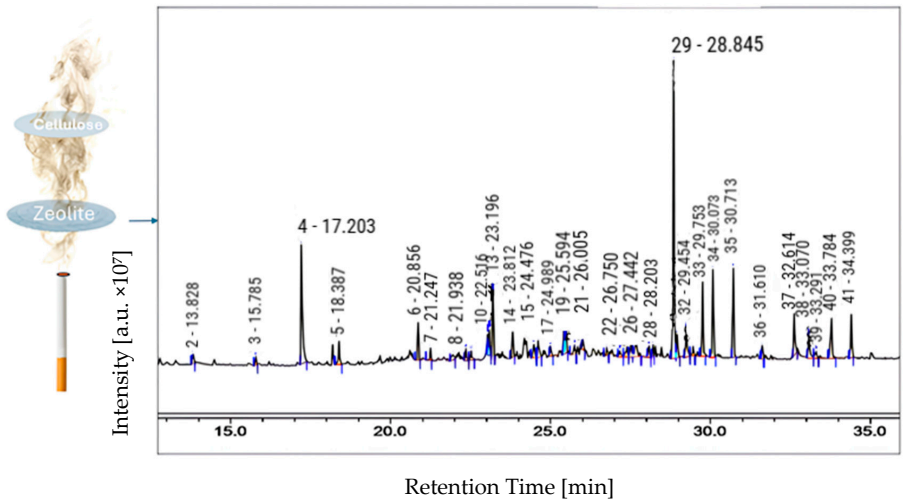

Figure 12. Enlargement of the region between 10.0 and 35.0 min of the gas-chromatogram of the extracts obtained from the zeolite composite filter. Assignment of peaks is as follows: 2, 2-phenoxyethanol; 3, dodec-1-ene; 4, nicotine; 5, tetradecane; 6, heptadecane; 7, 1,2-benzendiol; 8, eptadecene; 9, unknown; 10, docotriacontane; 11 and 12, unknown; 13, hexadecane; 14, dodecanoic acid methyl ester; 15, unknown; 16, 2-methyl-hexadecan-1-ol; 16, methyl hexadecanoate; 17, dibutyl phthalate; 18, unknown; 19, (Z)-2-(9-octadecenyloxy)-ethanol; 20 nonadecane; 21, tert-hexadecanthiol; 22, 23, 24, 25 and 26, unknown; 27, 1-nonadecene; 28, unknown; 29, phthalic acid; 30, methyl stearate; 31, hexadecanol; 32, docosyl ottyl ether; 33, 1-methyldodecyl benzene; 34, methyl hexadecanoate; 35, triphenylmethane; 36, unknown; 37, (Z)-11-hexadecen-1-ol; 38, dibutyl phthalate; 39, unknown; 40, octadecenoic acid methyl ester; 41, unknown.

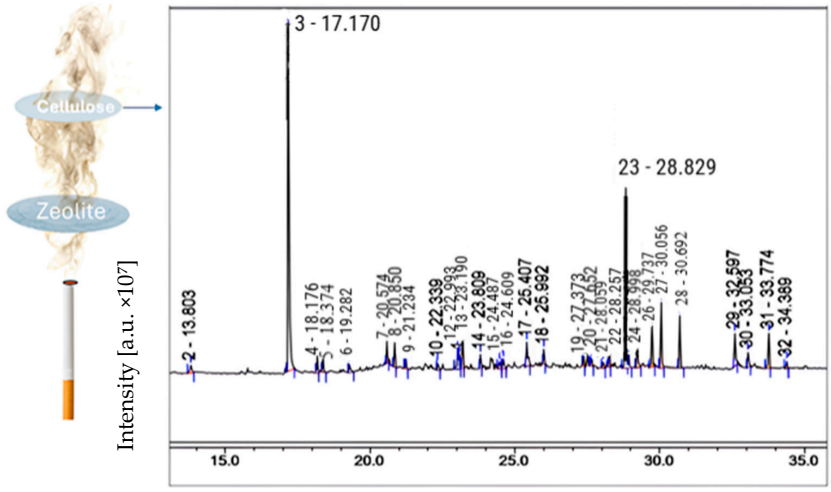

Figure 13. Enlargement of the region between 10.0 and 35.0 min of the gas-chromatogram of the extracts obtained from the cellulose used for the experiment performed with the zeolite composite filter. Assignment of peaks is as follows: 2, phenoxyethanol; 3, nicotine; 4, unknown; 5, tetradecane; 6, myosmine; 7, benzophenone; 8, eptadecane; 9, 1,2-benzendiol; 10, docotriacontane; 11 and 12, unknown; 13, hexadecane; 14, dodecanoic acid methyl ester; 15, unknown; 16, 2-methyl-1-hexadecanol; 17, nonadecane; 18, tert-hexadecanethiol; 19, 1-nonadecene; 20 and 2, unknown; 22, (Z)-2-(9-octadecyloxy)-ethanol; 23, phthalic acid; 24, unknown; 25, hexadecanol; 26, (1-methyldodecyl)-benzene; 27, hexadecanoic acid methyl ester; 28, triphenylmethane; 29, (Z)-11-hexadecen-1-ol; 30, dibutyl phthalate; 31, octadecenoic acid methyl ester; 32, unknown.

Furthermore, the extract obtained from the cellulose filter shows appreciable concentrations of various aromatic and phenolic compounds, as well as phthalates and long-chain alcohols. The presence of these substances in the extract suggests that the zeolite does not exhibit high efficiency in adsorbing aromatic and phenolic molecules, which represent a relevant and toxicologically significant fraction of cigarette smoke.

A comparative evaluation of the results obtained for the zeolite with those previously reported for carbon nanotubes (CNTs) [24] was also undertaken. Figures 14 and 15 present the chromatograms corresponding to the comprehensive analysis of an optimized experiment performed with CNTs under experimental conditions closely matching those adopted for the zeolite-based systems.

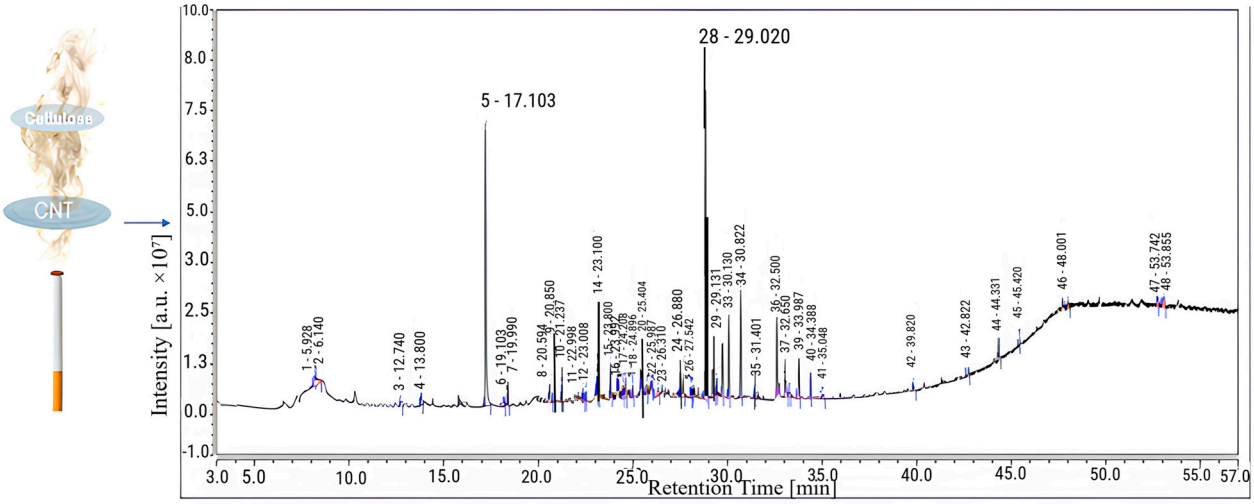

Figure 14. Total gas-chromatogram of the extract obtained from a typical experiment performed with the CNT filter. The two markers nicotine and phthalic acid generated peaks 5 and 28.

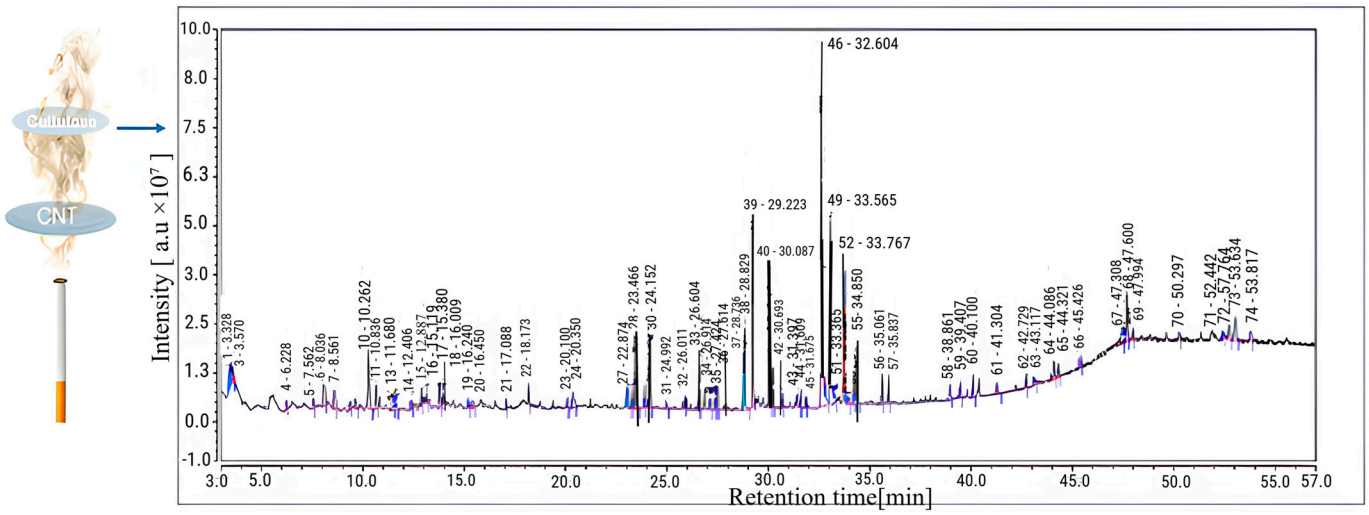

Figure 15. Total gas chromatogram of the extracts obtained from the cellulose filter used for the experiment performed with the cigarette filter loaded with CNT. Peaks of nicotine and phthalic acid were not detected.

In the case of CNTs, the chromatogram of the extract obtained from the carbon-based filter exhibits a highly complex profile, with numerous retained compounds. Nicotine represents the base peak of the chromatogram, and polycyclic aromatic hydrocarbons (PAHs), esters, alkenes, alkanes, and phthalates are also clearly detected. Another significant peak corresponds to phthalic acid, highlighting the strong adsorption capacity of CNTs toward this aromatic compound as well. The chromatogram of the extract obtained from the

cellulose filter associated with the CNT experiment is characterized by the absence of the peak attributable to nicotine, confirming the near-complete adsorption of this compound by the CNT-based filter. Moreover, the cellulose extract shows a marked reduction in the concentration of residual organic compounds, with only low-intensity peaks detected for the remaining species. The overall behavior observed in the experiments conducted with zeolite and, by comparison, with CNTs indicates that CNTs not only retain nicotine more efficiently than zeolite, but also exhibit a greater adsorption capacity toward aromatic and phenolic compounds, as well as long-chain hydrocarbons. This results in a significant reduction in the number of substances reaching the second filtration stage.

The comparison between zeolite and CNTs highlights clear differences, while also underscoring some positive aspects of the zeolite, such as its effective adsorption of phthalic acid. For aromatic and phenolic compounds, CNTs demonstrate superior adsorption performance, with minimal residual concentrations detected on the cellulose filter. Although zeolite retains these compounds to a lesser extent, its behavior is consistent with its crystalline framework and pore size distribution, which favor interactions with molecules of specific size and polarity. Overall, CNTs represent the most efficient filtering material among those investigated. Nevertheless, zeolite exhibits noteworthy selective adsorption properties that may be advantageous in targeted applications aimed at removing specific classes of volatile and semi-volatile compounds that are harmful to human health.

4. Conclusions

GC–MS analyses provided decisive insight into the selective nature of the adsorption processes. Zeolite A exhibited a pronounced affinity toward polar and oxygenated compounds, particularly phthalic acid, which was effectively retained. This behavior is consistent with the aluminosilicate nature of the LTA framework, characterized by polar sites and a well-defined pore size distribution that promotes interaction with molecules of specific dimensions and polarity. Although nicotine retention was significant, it was not complete, and the efficiency in trapping aromatic and phenolic compounds appeared more limited. This observation should not be interpreted solely as a weakness, but rather as an expression of the intrinsic selectivity of the material, governed by its crystalline structure and by electrostatic and molecular adsorption mechanisms. In contrast, CNTs, owing to their high specific surface area, mesoporous structure, and extended π-electron systems, exhibit broader and less selective interactions with various classes of organic compounds, including polycyclic aromatic hydrocarbons, phenols, and esters. The near-complete removal of nicotine and the marked reduction in residual organic species in the second filtration stage confirm a higher and more generalized adsorption efficiency.

In direct comparison, CNTs therefore emerge as the more effective material for the overall removal of particulate matter and a wide spectrum of volatile and semi-volatile organic compounds. Nevertheless, the present study demonstrates that zeolite should not be regarded as an intrinsically less efficient alternative, but rather as a selectively active adsorbent, particularly effective toward specific classes of polar molecules, including oxygenated compounds such as phthalic acid. The thermal and chemical stability of zeolite, combined with the possibility of tuning its cationic composition and pore architecture, further opens prospects for targeted optimization of its adsorption properties.

Overall, the results suggest that integrating materials with complementary properties, such as zeolites and CNTs, could represent a promising strategy for the design of multistage filtration systems capable of maximizing the removal of the different chemical fractions present in combustion smoke, combining high particulate retention capacity with tailored molecular selectivity. Beyond its technological relevance, the present study also holds environmental and public health significance. The reduction in volatile and semi-volatile

organic compounds, aromatic species, and fine particulate matter constitutes a priority objective for decreasing the environmental impact of combustion emissions and mitigating exposure to toxicologically relevant substances. Identifying filtering materials capable of selectively reducing specific classes of harmful compounds therefore contributes to the development of more effective strategies for controlling airborne pollutants.

The findings further highlight the potential for future developments, particularly through the design of hybrid systems combining zeolites and carbon nanotubes in structurally optimized configurations. Such an approach could synergistically exploit the high global adsorption efficiency of CNTs and the molecular selectivity of zeolites, paving the way for the development of more efficient, tunable, and sustainable filtration devices.

Author Contributions: Conceptualization, L.M., P.D.L., A.M. and C.S. Methodology, L.M. and P.D.L.; Formal analysis, P.F., L.M. and A.P.; Investigation, L.M., C.S., P.D.L. and A.M. Data curation, P.F., L.M. and A.P. Writing—original draft preparation, L.M. and P.D.L. Writing—review and editing, L.M., P.D.L. and C.S. Supervision, P.D.L., C.S. and L.M. All authors have read and agreed to the published version of the manuscript.

Funding: This research received no external funding.

Institutional Review Board Statement: Not applicable.

Informed Consent Statement: Not applicable.

Data Availability Statement: The data presented in this study are available on request from the corresponding author.

Conflicts of Interest: The authors declare no conflicts of interest.

References

1. Afolalu, E.F.; Spies, E.; Bacso, A.; Clerc, E.; Abetz-Webb, L.; Gallot, S.; Chrea, C. Impact of Tobacco and/or Nicotine Products on Health and Functioning: A Scoping Review and Findings from the Preparatory Phase of the Development of a New Self-Report Measure. *Harm Reduct. J.* **2021**, *18*, 79. [CrossRef] [PubMed]
2. Emma, R.; Caruso, M.; Campagna, D.; Pulvirenti, R.; Li Volti, G. The Impact of Tobacco Cigarettes, Vaping Products and Tobacco Heating Products on Oxidative Stress. *Antioxidants* **2022**, *11*, 1829. [CrossRef] [PubMed]
3. Dai, X.; Gakidou, E.; Lopez, A.D. Evolution of the Global Smoking Epidemic over the Past Half Century: Strengthening the Evidence Base for Policy Action. *Tob. Control* **2022**, *31*, 129–137. [CrossRef]
4. Kaunelienė, V.; Meišutovič-Akhtarieva, M.; Martuzevičius, D. A Review of the Impacts of Tobacco Heating System on Indoor Air Quality versus Conventional Pollution Sources. *Chemosphere* **2018**, *206*, 568–578. [CrossRef] [PubMed]
5. Varghese, J.; Muntode Gharde, P. A Comprehensive Review on the Impacts of Smoking on the Health of an Individual. *Cureus* **2023**, *15*, e46532. [CrossRef]
6. Agraval, H.; Yadav, U.C.S. Molecular Mechanisms of Passive Smoking-Induced Respiratory Diseases. *Respir. Med.* **2025**, *247*, 108279. [CrossRef]
7. Beutel, M.W.; Harmon, T.C.; Novotny, T.E.; Mock, J.; Gilmore, M.E.; Hart, S.C.; Traina, S.; Duttagupta, S.; Brooks, A.; Jerde, C.L.; et al. A Review of Environmental Pollution from the Use and Disposal of Cigarettes and Electronic Cigarettes: Contaminants, Sources, and Impacts. *Sustainability* **2021**, *13*, 12994. [CrossRef]
8. Cecinato, A.; Bacaloni, A.; Romagnoli, P.; Perilli, M.; Balducci, C. Indexes of Tobacco Smoke Contribution to Environmental Particulates Based on Molecular Fingerprints of Alkanes. *Environ. Sci. Pollut. Res.* **2022**, *29*, 43048–43057. [CrossRef]
9. Soleimani, F.; Dobaradaran, S.; De-la-Torre, G.E.; Schmidt, T.C.; Saeedi, R. Content of Toxic Components of Cigarette, Cigarette Smoke vs. Cigarette Butts: A Comprehensive Systematic Review. *Sci. Total Environ.* **2022**, *813*, 152667. [CrossRef]
10. Rodgman, A.; Smith, C.J.; Perfetti, T.A. The Composition of Cigarette Smoke: A Retrospective, with Emphasis on Polycyclic Components. *Hum. Exp. Toxicol.* **2000**, *19*, 573–595. [CrossRef]
11. Li, Y.; Hecht, S.S. Carcinogenic Components of Tobacco and Tobacco Smoke: A 2022 Update. *Food Chem. Toxicol.* **2022**, *165*, 113179. [CrossRef]
12. Qin, L.; Li, J.; Rui, J.; Zhu, Y.; Ren, H.; Zhu, C.; Zhai, H. Cellulosic Cigarette Papers: A Review of the Composition, Combustion Behavior, and Impact on Toxicant Release in Smoke. *J. Anal. Appl. Pyrolysis* **2026**, *193*, 107396. [CrossRef]

13. Asfaw, S.M.; Vijayawada, S.M.; Sharifian, Y.; Choudhry, F.; Khattar, P.; Cavalie, P.C.; Malasevskaia, I.; Vegiraju, S.M. Protecting Young Lives: A Systematic Review of the Impact of Secondhand Smoke Exposure and Legislative Measures on Children's Health. *Cureus* **2024**, *16*, e72548. [CrossRef] [PubMed]
14. Chan, S.S.C.; Cheung, Y.T.D.; Leung, D.Y.P.; Mak, Y.W.; Leung, G.M.; Lam, T.H. Secondhand Smoke Exposure and Maternal Action to Protect Children from Secondhand Smoke: Pre- and Post-Smoke-Free Legislation in Hong Kong. *PLoS ONE* **2014**, *9*, e105781. [CrossRef]
15. Boderie, N.W.; Sheikh, A.; Lo, E.; Sheikh, A.; Burdorf, A.; van Lenthe, F.J.; Mölenberg, F.J.M.; Been, J.V. Public Support for Smoke-Free Policies in Outdoor Areas and (Semi-)Private Places: A Systematic Review and Meta-Analysis. *eClinicalMedicine* **2023**, *59*, 101982. [CrossRef]
16. Wei, H.; Rui, J.; You, M.; Wang, X.; Li, J.; Zhu, C.; Ma, M. Materials for the Selective Removal of Toxic Compounds in Cigarette Smoke: A Review. *Sep. Purif. Technol.* **2025**, *354*, 128908. [CrossRef]
17. Zhou, S.; Fu, Z.; Xia, L.; Mao, Y.; Zhang, C.; Chen, J. Blocking and Filtering Effect of Filter Tips of Natural Fibers against Mainstream Cigarettes Smoke. *J. Nat. Fibers* **2021**, *18*, 2327–2337. [CrossRef]
18. Han, S.; Kim, J.; Ko, S.H. Advances in Air Filtration Technologies: Structure-Based and Interaction-Based Approaches. *Mater. Today Adv.* **2021**, *9*, 100134. [CrossRef]
19. De Luca, P.; Siciliano, C.; Macario, A.; Nagy, J.B. The Role of Carbon Nanotube Pretreatments in the Adsorption of Benzoic Acid. *Materials* **2021**, *14*, 2118. [CrossRef] [PubMed]
20. Wang, L.; Zhu, F.; Liu, E.; Yang, Y.; Yu, Q.; He, Y.; Peng, W.; Lam, S.S.; Chen, X. Progress in Advanced Carbon Nanotubes Composites for Air Purification. *Adv. Compos. Hybrid Mater.* **2024**, *7*, 100. [CrossRef]
21. De Luca, P.; Macario, A.; Siciliano, C.; B.Nagy, J. Recovery of Biophenols from Olive Vegetation Waters by Carbon Nanotubes. *Materials* **2022**, *15*, 2893. [CrossRef] [PubMed]
22. De Luca, P.; Macario, A.; Madeo, L.; B.Nagy, J. The Influence of Carbon Nanotube Functionalization on Water Contaminated by Diesel and Benzoic Acid: A Comparison of Two Case Studies. *Inorganics* **2024**, *12*, 238. [CrossRef]
23. Vishwakarma, P.K.; Pandey, S.K.; Singh, A.K.; Rathore, S.; Ram, K.; Giri, R.; Srivastava, A. Reusable and Thermostable Multiwalled Carbon Nanotubes Membrane for Efficient Removal of Benz[α]anthracene from Cigarette Smoke. *Oxf. Open Mater. Sci.* **2023**, *3*, itad012. [CrossRef]
24. Madeo, L.; Figliuzzi, P.; Perri, A.; Macario, A.; Siciliano, C.; De Luca, P. Carbon Nanotube-Based Filters for the Adsorption of Toxic Compounds in Cigarette Smoke. *C* **2026**, *12*, 8. [CrossRef]
25. Vuono, D.; De Luca, P.; Nagy, J.B.; Nastro, A. Synthesis and characterization of self-bonded ETS-4 and ETS-10 pellets. *Microporous Mesoporous Mater.* **2008**, *109*, 118–137. [CrossRef]
26. Gatta, G.D.; Lotti, P. Systematics, Crystal Structures, and Occurrences of Zeolites. In *Modified Clay and Zeolite Nanocomposite Materials*; Mercurio, M., Sarkar, B., Langella, A., Eds.; Micro and Nano Technologies; Elsevier: Amsterdam, The Netherlands, 2019; pp. 1–25. [CrossRef]
27. Vuono, D.; Guzzo, M.; De Luca, P.; Nagy, J.B. Physico-chemical characterisation of zirconium-based self-bonded ETS-4 pellets. *J. Therm. Anal. Calorim.* **2014**, *116*, 169–182. [CrossRef]
28. Madeo, L.; Blom, N.; Joensen, F.; Nagy, J.B.; De Luca, P. Steam-Induced Aluminum Speciation and Catalytic Enhancement in ZSM-5 Zeolites. *Catalysts* **2025**, *15*, 1130. [CrossRef]
29. Kordala, N.; Wyszkowski, M. Zeolite Properties, Methods of Synthesis, and Selected Applications. *Molecules* **2024**, *29*, 1069. [CrossRef] [PubMed]
30. Parmar, M.; Shahabuddin, S.; Bandyopadhyay, M.; Gaur, R. Zeolites in the Age of Advanced Materials: From Structural Refinement to Scalable Green Synthesis and Emerging Applications. *Emergent Mater.* **2025**, *8*, 4063–4107. [CrossRef]
31. Marcilla, A.; Berenguer, D.; Martinez, I. Effect of the Addition of Zeolites and Silicate Compounds on the Composition of the Smoke Generated in the Decomposition of Heet Tobacco under Inert and Oxidative Atmospheres. *J. Anal. Appl. Pyrolysis* **2022**, *164*, 105532. [CrossRef]
32. Marcilla, A.; Berenguer, D.; Beltrán, M.I.; Farcas, C. Catalytic Reduction of the Compounds Generated When Heating Heet Tobacco in Presence of USY and Beta Zeolites and Silica Lovel 6000 and SBA-15 Silicate in Oxidative and Inert Atmospheres: Effect of Temperature and Catalyst Content. *ChemEngineering* **2024**, *8*, 125. [CrossRef]

Disclaimer/Publisher's Note: The statements, opinions and data contained in all publications are solely those of the individual author(s) and contributor(s) and not of MDPI and/or the editor(s). MDPI and/or the editor(s) disclaim responsibility for any injury to people or property resulting from any ideas, methods, instructions or products referred to in the content.